

Computational Quantum Chemistry on the Photoelectric Characteristics of Semiconductor Quantum Dots and Biological Pigments

Che-Wun Hong^{1,2} and Wei-Hui Chen¹

Abstract: This paper intends to use semiconductor quantum dots (cadmium sulphide-CdS) and/or biological pigments (chlorophyll-*a* derivatives) to replace those expensive ruthenium (Ru) dyes in photoelectrochemical solar cells. Based on the computational quantum chemistry, the molecular structures of $(\text{CdS})_n$ ($n=1\sim 22$) clusters and chlorophyll-*a* derivatives (chlorin- H_3^+ and chlorin- H_{17}^+) are configured and optimized. Density functional theory (DFT) of the first principles calculations, which chose B3LYP (Becke 3-parameter Lee-Yang-Parr) and PBE (Perdew-Burke-Ernzerhof) exchange correlation functionals, is employed. Photoelectric properties, such as: molecular orbital, density of state (DOS), highest occupied molecular orbital (HOMO), lowest unoccupied molecular orbital (LUMO) and resultant band gaps are predicted. The band gaps calculated from the computer modeling are close to experiments. It is concluded that we can enhance the sunlight absorption by mixing different diameters of semiconductor quantum dots. Also biological pigment, chlorin- H_3^+ , has a suitable bonding structure with the TiO_2 electrode. Broad light absorption spectra and cheap price are their major characteristics.

Keywords: computational quantum chemistry, quantum dots, biological pigments

1 Introduction

In the quantum dot-sensitized solar cell (QDSSC) research, the II-VI and III-V groups, such as: CdS (Peter, Riley, Tull and Wijayantha, 2002), CdSe (Robel, Subramanian, Kuno, and Kamat, 2006), InP (Blackburn, Selmarten, Ellingson, Jones, Micic, and Nozik, 2005) and others (Schaller and Klimov, 2004; McDonald, Konstantatos, Zhang, Cyr, Klem, Levina, and Sargent, 2005), are popular materials for

¹ Department of Power Mechanical Engineering, National Tsing Hua University, Hsinchu 30013, Taiwan

² Corresponding author. Phone: +886-3-5742591; Fax: +886-3-5722840; E-mail: cwhong@pme.nthu.edu.tw

sensitizers because of their ability to harvest light energy ranges from ultraviolet to even infrared (Yoshino, Lee, Fujii, Nakayama, Schneider, Naka, and Ishikawa, 1999). This ability is attributed to their energy gaps, which are controllable and normally are lower than those of semiconductor bulk materials. Hotchandani and Kamat (1992) used a ZnO electrode to coat with CdS quantum dots as sensitizers, which could achieve 15% quantum efficiency when the solar cell was illuminated with the visible light (wavelength > 420 nm) from a halogen lamp. Plass, Pelet, Krueger and Grätzel (2002) used PbS quantum dots and TiO₂ electrode to fabricate a high quantum efficiency (45%) QDSSC, whose photovoltaic performance could obtain 0.49% at AM1.5. A few years later, Lee, Yum, Leventis, Zakeeruddin, Haque, Chen, Seok, Grätzel and Nazeeruddin (2008) fabricated a new QDSSC using CdSe quantum dots which could achieve a photovoltaic performance greater than 1% at full-sun intensity. In 2005, Zeng, Schelly, Noto and Marynick (2005) used density functional theory to study the structures of lead sulfide clusters, (PbS)_n (n = 1-9), and calculated their energy gaps. Matxain, Mercero, Fowler and Ugalde (2004) calculated the energy gaps of clusters of II-VI materials: Cd_iX_i (where X=S, Se and Te with i<16) and concluded that the energy gaps were lower in three-dimensional structure than those in the two-dimensional configuration. As the cluster diameter decreases, the energy gap increases.

Regarding biological pigments, Tennakone and Kumarasinghe (1997) investigated the flower pigment cyanidin as a sensitizer and found that it anchored into nanoporous films of TiO₂ by surface complexation and generated high photocurrent of good stability. Hara and Kurashige (2003) designed new coumarin dyes and proposed new pigments, named NKX-2311, NKX-2593 and NKX-2677. Among these organic sensitizers, the NKX-2677 could achieve a 7.7% photovoltaic performance. Wang and Sasaki (2010) investigated the electron injection and charge collection processes in chlorophyll-*a* derivatives with various hydrocarbon ester groups which gave a solar energy-to-electricity conversion efficiency up to 8%.

Currently, the overall performances of both QDSSCs and biological pigment solar cells are still lower than traditional Ru-based dye-sensitized solar cells (DSSCs). The research is still ongoing because both quantum dots and biological pigments are cheaper and their band gaps are controllable. The objective of this paper is to use computational quantum chemistry to perform quantum analysis and to observe the photoelectric effects due to molecular structure variations. Finding their best positions for an easier connection with the photo-anode is also critical. The following sections will describe the computer modeling to predict the photoelectric characteristics of example quantum dots and biological pigments.

2 Computational Quantum Chemistry

Computational quantum chemistry (Levine, 2009; Lewars, 2003) is a powerful tool for modern nanotechnologies (Srivastava, Atluri, 2002; Fitzgerald, Goldbeck-Wood, Kung, Petersen, Subramanian, Wescott, 2008). It mainly uses electronic structure modeling to investigate the photo-electrochemical phenomena of interest in this paper. The calculation is based on the first principles of physics, namely: *ab initio*, semi-empirical, molecular mechanics, and density functional theory (DFT) (Leach, 2001). This paper focused on the DFT, which is based not on the wave function Ψ , but rather on the electron probability density function, designated by ρ . For a system of n electrons, $\rho(\vec{r})$ denotes the total electron density at a particular position \vec{r} in space. The electronic energy, denoted by $E[\rho]$, is said to be a functional of the electron density. There is a single corresponding electronic energy $E[\rho]$ for a given function $\rho(\vec{r})$. The exact electron density and the electronic energy are expressed by

$$\rho(\vec{r}) = \sum_i^n |\psi_i(\vec{r})|^2 \quad (1)$$

$$E[\rho(\vec{r})] = E_T[\rho(\vec{r})] + E_V[\rho(\vec{r})] + E_J[\rho(\vec{r})] + E_{XC}[\rho(\vec{r})] \quad (2)$$

where E_T is the kinetic energy term arisen from the motion of the electrons; E_V includes terms describing the potential energy of the nuclear-electron attraction and the repulsion between pairs of nuclei; E_J is the electron-electron repulsion term; and E_{XC} represents the exchange-correlation term which includes the remaining part of the electron-electron interactions. The major problem in the DFT is that the exact functionals for the exchange-correlation term are not known except for the free electron gas. In our simulation, we adopted the well-known B3LYP approximation (Foresman, Frisch, 1996), which pairs the Becke's gradient-corrected exchange functional with the gradient-corrected correlation functional of Lee, Yang and Parr (1988). This hybrid exchange-correlation functional is constructed as a linear combination of the Hartree-Fock exact exchange functional (E_X^{HF}) and a number of exchange and correlation explicit density functionals, which are expressed by:

$$E_{XC}^{B3LYP} = E_{XC}^{LDA} + a_0(E_X^{HF} - E_X^{LDA}) + a_x(E_X^{GGA} - E_X^{LDA}) + a_c(E_C^{GGA} - E_C^{LDA}) \quad (3)$$

where $a_0 = 0.20$, $a_x = 0.72$, and $a_c = 0.81$ are three weighting coefficients, E_X^{GGA} and E_C^{GGA} are generalized gradient approximations (GGA) of the Becke exchange functional (Becke, 1988), and the correlation functional derived by Lee, Yang and

Parr (1988), and E_C^{LDA} is the VWN (Vosko, Wilk, Nusair, 1980) local-density approximation (LDA) to the correlation functional. The first step in the LDA is to calculate the density gradient function at every point. Many different GGA exchange-correlation approximations were proposed and PBE (Perdew, Burke, and Ernzerhof, 1996) approach was one of the favourite options for solids and gases (Hong and Tsai, 2010). It is expressed by

$$E_{XC}^{PBE} = \int d^3\vec{r} \rho(\vec{r}) E_{XC}^{unif} F_{XC} \quad (4)$$

where the exchange correlation energy per particle of a uniform electron gas, E_{XC}^{unif} , was well established by Perdew and Wang (1992) and the enhancement factor, F_{XC} , was also derived by Perdew and his colleagues (Perdew, Chevary, Vosko, Jackson, Pederson, Singh, and Fiolhais, 1992).

3 Quantum Dots

3.1 Geometry Optimization

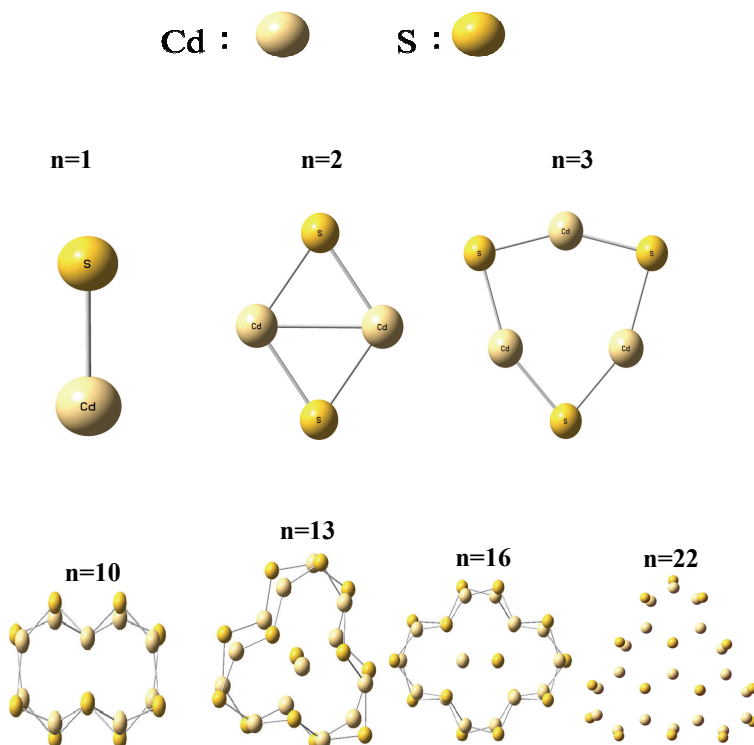
Although there are many kinds of semiconductor quantum dots composed by III-V and II-VI groups, we choose the cadmium-sulphide (CdS) clusters as the first example to start with our study. The material property table shows that the conduction band of the CdS is slightly higher than the TiO₂ electrode's conduction band; that makes the hot electron injection possible from the sensitizer to the electrode (Grätzel, 2001). Decreasing the size of the CdS particles to quantum scale is expected to increase the band gap (and also the conduction band potential) due to the quantum confinement effects. A quantum chemistry software, Gaussian 09 (G09), was employed in this study as the simulation platform (Frisch et al, 2009). The first step was to optimize the molecular structures of clusters (CdS)_n (n=1~22) by minimizing the total energy of each configuration. Table 1 shows the total energy at the optimized geometry using different exchange correlation functionals. It is observed that the two different approximations, G09-PBE and G09-B3LYP, have almost the same total energy. In addition, with increase of the repetition "n" number, the total energy decreases and represents stable trend. Figure 1 plots the optimized geometries of (CdS)_n clusters, composed by a number of rings and layers as n increases. According to the calculation results, the optimized geometries are not exactly wurtzite structure but still are composed by hexagonal rings.

3.2 Photoelectric Analysis

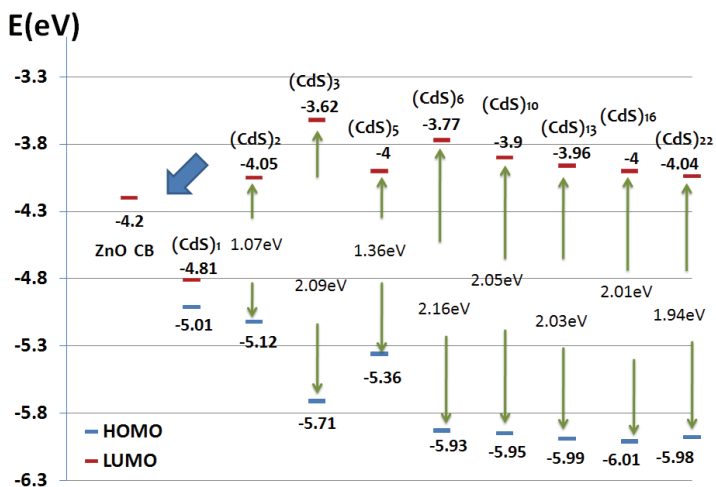
In computational quantum chemistry, the major photoelectric property- band gaps can be obtained from the potential difference between the lowest unoccupied molecular orbital (LUMO) and the highest occupied molecular orbital (HOMO). Figure 2

Table 1: Total energy of $(\text{CdS})_n$ ($n=1\sim 22$) using different exchange-correlation functionals

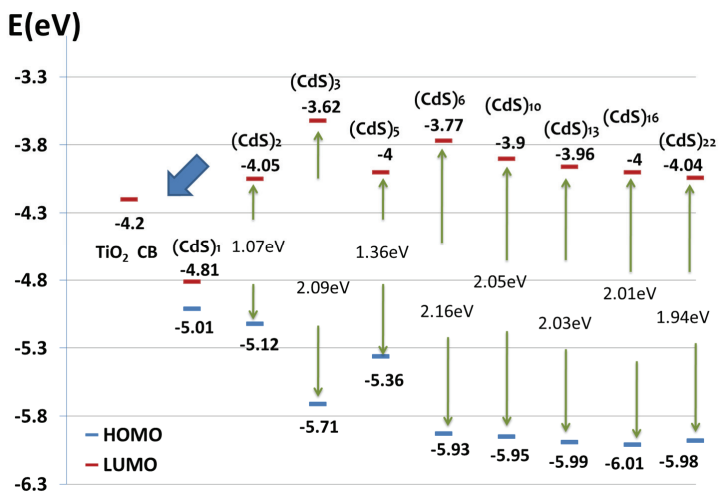
Total energy	$(\text{CdS})_1$	$(\text{CdS})_2$	$(\text{CdS})_3$	$(\text{CdS})_{10}$
G09-PBE	-58.36	-116.86	-175.37	-584.86
G09-B3LYP	-58.13	-116.39	-174.69	-582.51
	$(\text{CdS})_{13}$	$(\text{CdS})_{16}$	$(\text{CdS})_{22}$	unit: Hartree
G09-PBE	-760.36	-935.86	-1286.86	
G09-B3LYP	-757.3	-932.1	-1281.69	

Figure 1: Geometry optimization of clusters $(\text{CdS})_n$ ($n=1\sim 22$)

shows that using both G09-B3LYP and G09-PBE approximations can achieve similar trend but different absolute values of potential energies. It can be noted that all LUMOs are higher than the conduction band (CB) of the TiO_2 except $(\text{CdS})_1$. As n decreases from 22 to 6, the HOMO and the LUMO potentials have an increasing trend, and the band gaps between them also increase. The quantum confinement ef-



(a) G09-B3LYP



(b) G09-PBE

Figure 2: Band gaps between LUMOs and MOMOs of clusters $(CdS)_n$ using (a) G09-B3LYP and (b) G09-PBE methods. All LUMOs are higher than the conduction band (CB) of the TiO_2 except $(CdS)_1$ which impedes electron injection.

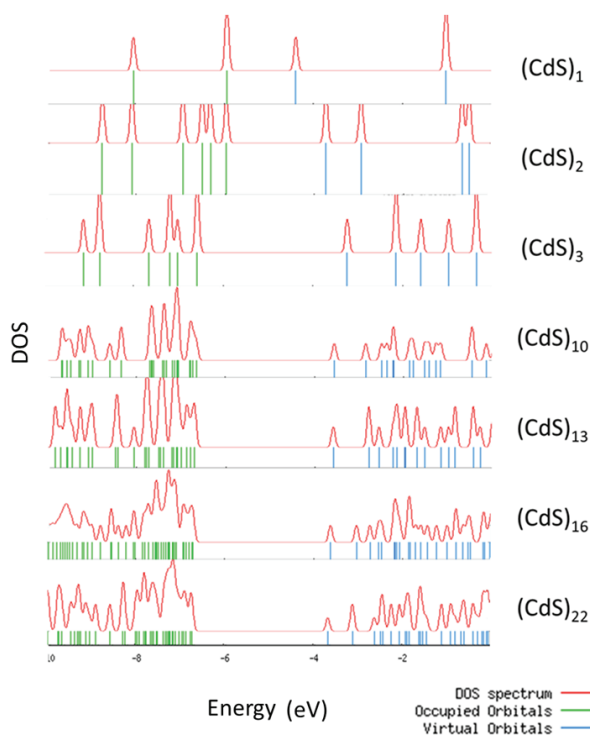


Figure 3: Density of state (DOS) diagram of $(\text{CdS})_n$. Because of the Pauli's uncertainty principle, electrons in bigger size clusters will tend to aggregate in both LUMO and HOMO that makes the band gap evaluation more meaningful. When the cluster number decreases, the electrons will be more dispersed and that causes the DOS also more dispersed.

fect is exhibited clearly in such scale of the quantum dots. However, when the size of the clusters continues to decrease, the LUMOs start to fluctuate, even decrease below the CB of the electrode that impedes electron injection. The reason can be explained from the density of state (DOS) diagram shown in Figure 3. Because of the Pauli's uncertainty principle, electrons in bigger size clusters will tend to aggregate in both LUMO and HOMO regimes that make the band gap evaluation more meaningful. When the cluster number (or the quantum dot diameter) continues to decrease, the electrons will be more dispersed and that makes the DOS diagram more dispersed as well. Figure 4 shows energy gaps of $(\text{CdS})_n$ predicted by B3LYP and PBE approximations. Comparison of simulation and experimental results indicates that the theoretical calculations tend to over-predict the energy gap values.

The experiment was carried out by Michalet, Pinaud, Bentolila, Tsay, Doose, Li, Sundaresan, Wu, Gambhir, and Weiss (2005). The measured and predicted energy gaps have the same trend, corresponding to the quantum confinement effect. The fluctuating regime is due to the dispersed electronic DOS when the cluster is too small.

Electron transfer takes place because of the LUMO and HOMO potentials; another factor is due to the HOMO-1, HOMO, LUMO and LUMO+1 interactions. From Figure 5, it can be observed that electrons are aggregated around the S atom at HOMO and HOMO-1. On the other hand, electrons are aggregated around the Cd atom at LUMO and LUMO-1 when they are excited. It was reported by Labat, Baranek, and Adamo (2008) that the conduction band of the TiO₂ is mainly on the Ti atom and its valence band is on the O atoms. Ti and S atoms may attract each other; S atoms play the role of the linkage atoms to the TiO₂ electrode. In fact, the electrons were aggregated more around the Cd atom at LUMO and LUMO-1, so the electrons won't inject easily into the TiO₂ conduction band. Even if some electrons successfully inject into the TiO₂ conduction band, they will quite possibly recombine with the holes in the HOMO. Because of the phenomena, it can be concluded that the (CdS)_n clusters have not a suitable connection with the TiO₂ electrode. That makes the injection efficiency lower than expected and the linker structure still needs further improvement using modern nanotechnologies.

4 Biological Pigments

4.1 Geometry Optimization

Biologic pigments are natural sensitizers; they are easy to be extracted from plants and their quantum efficiencies can achieve 100% theoretically. Chlorophyll-*a* is a specific form of the chlorophyll used in oxygenic photosynthesis. It absorbs most energy from wavelengths of violet-blue and orange-red light. Our research starts from the most common chlorophyll-*a* derivatives (C₃₄H₃₀N₄O₅). The simulation system in this section consists of four molecular species, namely: hydrogen (H), carbon (C), oxygen (O) and nitrogen (N) atoms as shown in Figure 6(a). Figures 6 (b) and 6(c) show the optimized geometry of the sensitizer molecule, in which two carboxyl groups (COOH) locate at the #3 and the #17 positions, respectively.

4.2 Chlorin Proton Affinity

Figure 7 illustrates the top view and the side view of the optimized geometry of the chlorin-H₃⁺ in which an amount of energy is required to remove a proton at the #3 position. The optimized geometry of chlorin-H₁₇⁺ is shown in Figure 8, in which the proton is removed at the #17 position. These two de-protonation ge-

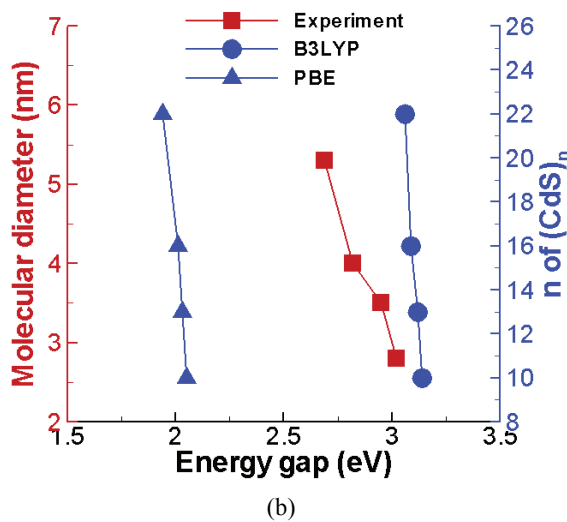
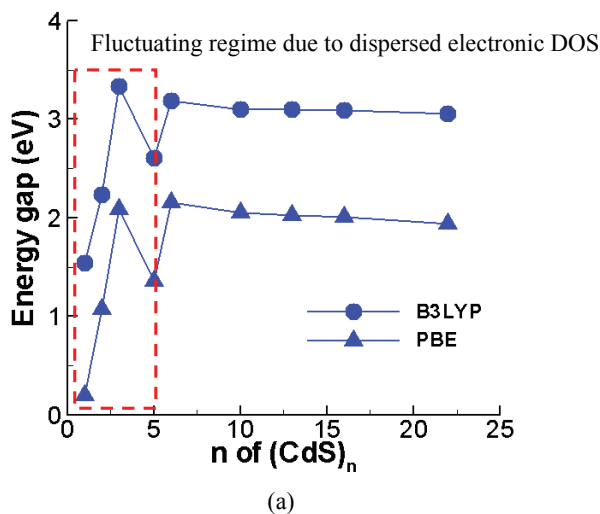


Figure 4: (a) Energy gaps of $(\text{CdS})_n$ predicted by B3LYP and PBE approximations, the fluctuating regime is due to the dispersed electronic DOS. (b) Comparison of simulation and experimental results indicates that the theoretical calculations well predicts the trend of the quantum confinement effect, but not the absolute values.

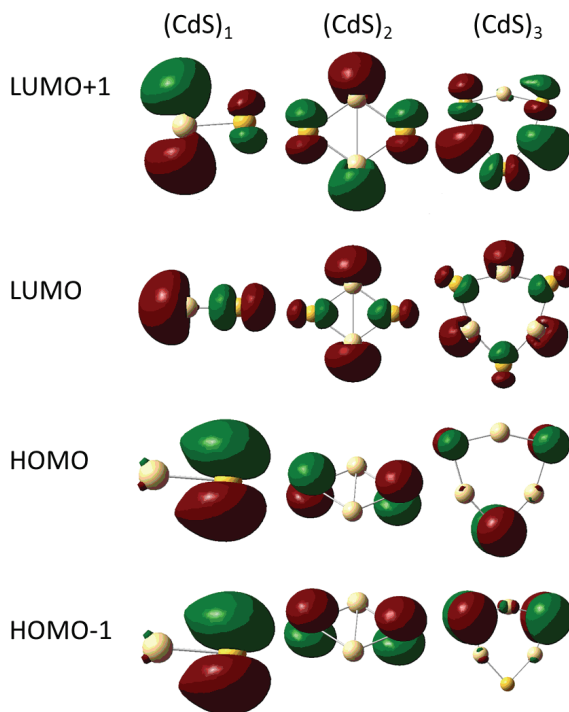


Figure 5: Molecular orbital diagrams of $(\text{CdS})_n$. Green color indicates electrons spin up and brown color means spin down. Electrons are aggregated around the S atom at HOMO and HOMO-1. On the other hand, electrons are aggregated around the Cd atom at LUMO and LUMO-1.

ometries have a central region that shows the same two-dimensional surface and a three-dimensional structure near the molecule's functional groups (COOH). Table 2 shows the proton affinities (PA) of the chlorin with different deprotonation configurations. The proton affinity values are equal to the chlorin molecule's total energy minus chlorin- H_3^+ (or chlorin- H_{17}^+) molecule's total energy. It can be seen that the energy required to form chlorin- H_3^+ is less than the chlorin- H_{17}^+ which means that it is easier for chlorin- H_3^+ to remove the proton and to bond with the TiO_2 electrode. This result has been experimentally verified by Wang and Sasaki (2010) that the chlorin-3 with a dodecyl ester group gave a stable linkage to the TiO_2 electrode and generated the highest solar energy-to-electricity conversion efficiency.

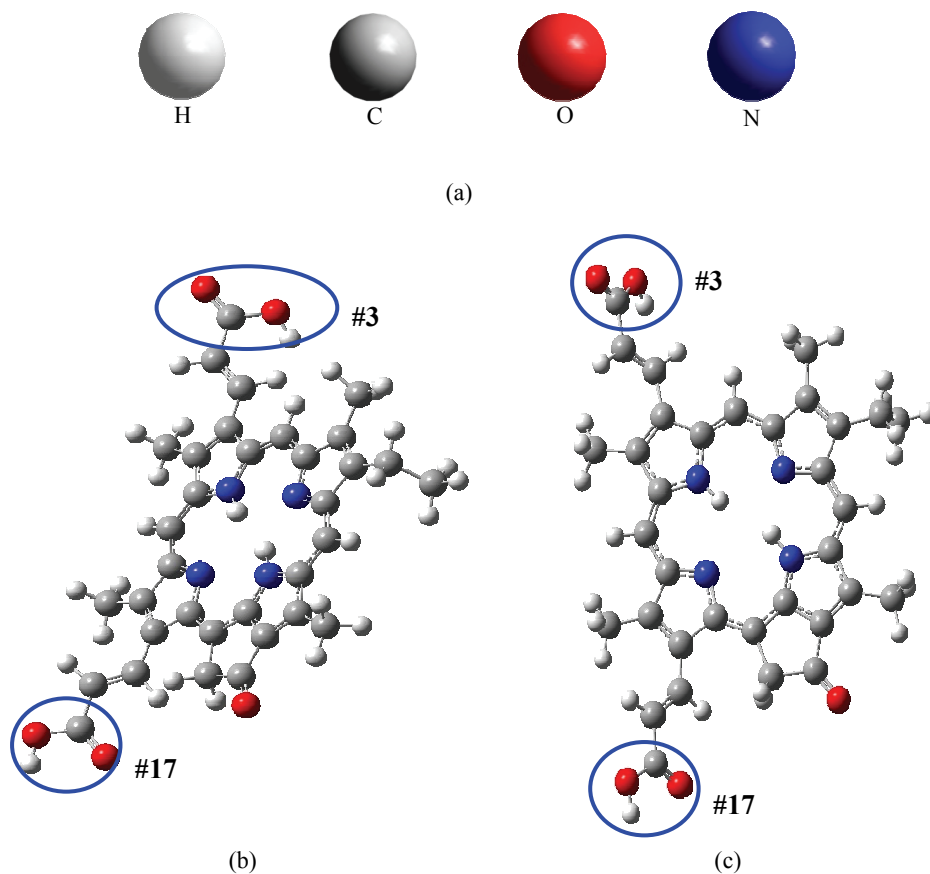


Figure 6: (a) Molecular species, (b) top view, and (c) side view of optimized geometry of chlorin ($C_{34}H_{30}N_4O_5$) molecules, in which two carboxyl groups (COOH) locate at the #3 and the #17 positions.

Table 2: Proton affinities for chlorin- H_3^+ and chlorin- H_{17}^+

Pigments	Proton affinity (PA)
Chlorin- H_3^+	334.650 Kcal-mol $^{-1}$
Chlorin- H_{17}^+	345.820 Kcal-mol $^{-1}$

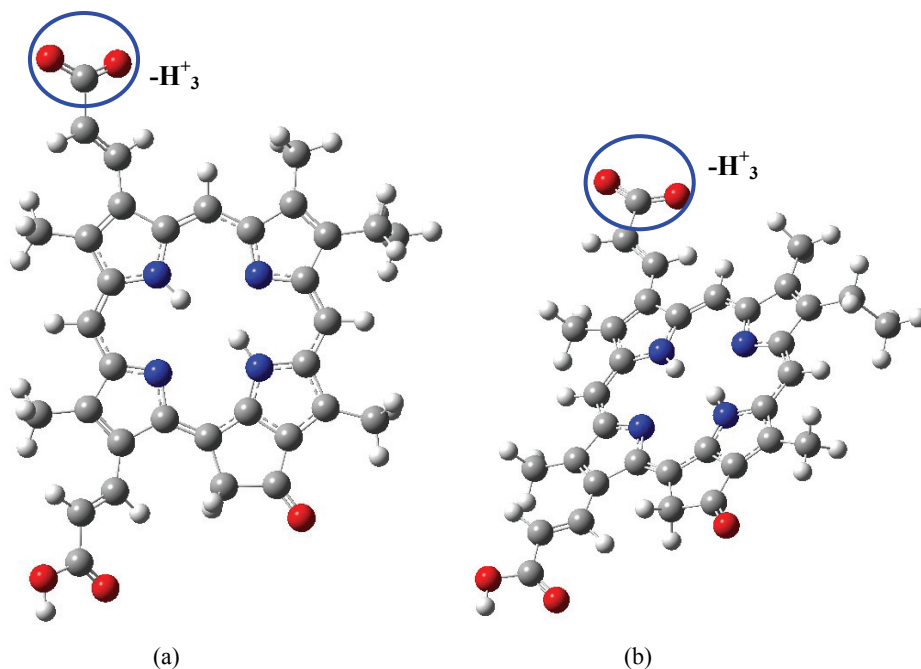


Figure 7: (a) Top view and (b) side view of optimized geometry of the chlorin- H_3^+ in which an amount of energy is required to remove a proton at the #3 position.

Table 3: Predicted energy gaps of chlorin- H_3^+ and chlorin- H_{17}^+

(Unit : eV)		Chlorin- H_3^+	Chlorin- H_{17}^+
Vacuum	HOMO	-3.0592	-2.9169
	LUMO	0.0941	-0.1741
	Band gap	3.1533	2.7427
Ethanol solvent	HOMO	-6.2844	-6.283
	LUMO	-1.7841	-1.8674
	Band gap	4.5002	4.4161

4.3 Chlorin Energy Gap

Figure 9 shows the predicted energy gaps of chlorin- H_3^+ and chlorin- H_{17}^+ under vacuum state and in the ethanol solvent. Table 3 tabulates their values for HOMOs, LUMOs, and band gaps. All the LUMOs of the chlorin molecules are higher than the conduction band of the TiO_2 electrode. Both chlorin- H_3^+ and chlorin- H_{17}^+ pig-

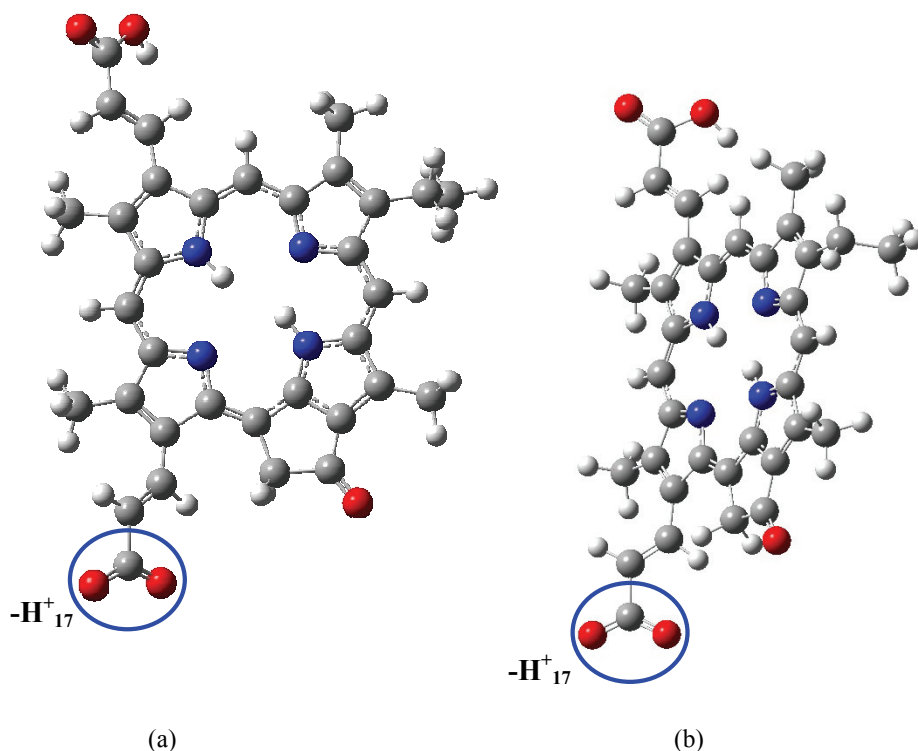


Figure 8: (a) Top view and (b) side view of optimized geometry of the chlorin- H_{17}^+ in which an amount of energy is required to remove a proton at the #17 position.

ments have lower LUMO and HOMO potentials under the solvent effect than in the vacuum state. However, chlorin- H_3^+ and chlorin- H_{17}^+ molecular energy gaps have a greater value in the solvent than in the vacuum state, which corresponds to the blue shift phenomenon with the solvent effect. Figure 10 shows the molecular orbital distribution diagrams of the chlorin sensitizer. When the chlorin is at the HOMO state, the electrons are distributed near the central region. When it is excited by visible light to the LUMO state, the electron distribution is directional to the #3 position. It has been explained that it is easier for chlorin- H_3^+ to bond with the TiO_2 electrode in the previous section; that means the chlorine- H_3^+ has the potential to have the least impedance in the electrolyte-dye-electrode interface which affects the electron injection and charge recombination subsequently. Both the energy level and the geometric connection between the sensitizers and the electrode affect the electron injection efficiency, which is the most important parameter in

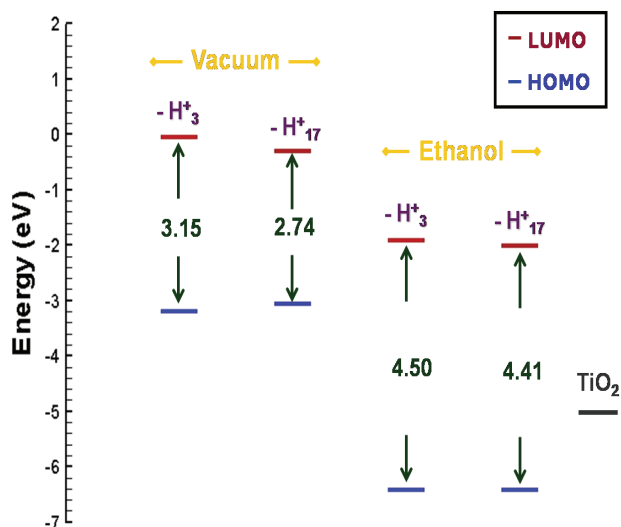


Figure 9: Energy gaps predicted for chlorin- H_3^+ and chlorin- H_{17}^+ under vacuum state and in the ethanol solvent. Blue shift phenomena can happen with the solvent effect. All the LUMOs of the chlorin sensitizers are higher than the conduction band of the TiO_2 electrode.

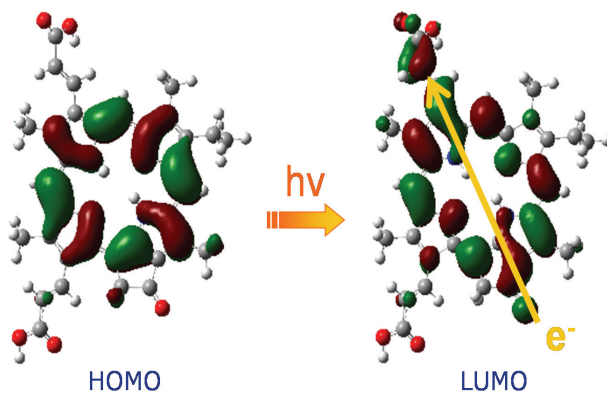


Figure 10: Molecular orbital distribution diagrams of the chlorin sensitizer. When it is at the HOMO state, the electrons are distributed near the central ring. When it is excited by visible light to the LUMO state, the electron distribution is directional to the #3 position, which is linked to the electrode.

the photoelectrochemical solar cell design.

5 Conclusions

The simulation results in this paper have concluded that both semiconductor quantum dots and biological pigments can be used to replace the traditional Ru-sensitizers in the photoelectrochemical solar cell design. In semiconductor quantum dots, the cluster number reduction, from $(\text{CdS})_{22}$ to $(\text{CdS})_{10}$, will increase the HOMO and LUMO potentials and exhibit the quantum confinement effect which has been confirmed experimentally. It has been revealed that S atoms acted as the bridge between the $(\text{CdS})_n$ sensitizer and the TiO_2 electrode. The linkage doesn't have a good connectivity because the Cd atom at LUMO and LUMO+1 conditions will not inject electrons easily into the TiO_2 conduction band via the S atoms. Therefore, $(\text{CdS})_n$ quantum dots are currently not a suitable sensitizer replacement, and they need further improvement at the linker structure through modern nanotechnologies. Computational quantum chemistry can do a great help for that.

Regarding the biologic pigments, two deprotonation geometries of the chlorin sensitizers have been studied in this paper. It was observed that they have a central region which exhibits a two-dimensional surface and a three-dimensional structure near the molecule's functional group to connect with the electrode. Chlorin- H_3^+ has an easier ability to bond with the TiO_2 because of the lower energy required to remove the hydrogen proton. Chlorin- H_3^+ and chlorin- H_{17}^+ energy gaps have a greater value in the ethanol solvent than under the vacuum state, which corresponds to the blue shift phenomenon under realistic environmental conditions. Both the energy level and the geometric connection between the chlorin and the electrode show that the biological pigment is an excellent alternative to the expensive Ru-sensitizers. Further investigations on fabrication of the biological solar cells are an interesting subject for future research.

Acknowledgement: Thanks are due to the National Science Council of Taiwan (NSC 98-2221-E-007-108-MY3) and National Tsing Hua University Boost Program (NTHU 99N2521E1) who supported this research with the grant to Mr. W. H. Chen. We are also grateful to the National Center for High-performance Computing (NCHC) for the generous computer time and facilities.

References

- Becke, A. D. (1988): Density-functional exchange-energy approximation with correct asymptotic behavior. *Phys. Rev. A*, vol. 38, pp. 3098–3100.
- Blackburn, J. L.; Selmarten, D. C.; Ellingson, R. J.; Jones, M.; Micic, O.;

Nozik, A. J. (2005): Electron and hole transfer from indium phosphide quantum dots. *J. Phys. Chem. B*, vol. 109, pp. 2625-2631.

Foresman, J. B.; Frisch, A. (1996): *Exploring Chemistry with Electronic Structure Methods*, 2nd Edition, Gaussian, Inc., Pittsburgh, PA.

Fitzgerald, G.; Goldbeck-Wood, G.; Kung, P.; Petersen, M.; Subramanian, L.; Wescott, J. (2008): Materials modeling from quantum mechanics to the mesoscale. *CMES: Computer Modeling in Engineering & Science*, vol. 24, pp. 169-183.

Frisch, M. J.; Trucks, G. W.; Schlegel, H. B.; Scuseria, G. E.; Robb, M. A.; Cheeseman, J. R.; Scalmani, G.; Barone, V.; Mennucci, B.; Petersson, G. A.; Nakatsuji, H.; Caricato, M.; Li, X.; Hratchian, H. P.; Izmaylov, A. F.; Bloino, J.; Zheng, G.; Sonnenberg, J. L.; Hada, M.; Ehara, M.; Toyota, K.; Fukuda, R.; Hasegawa, J.; Ishida, M.; Nakajima, T.; Honda, Y.; Kitao, O.; Nakai, H.; Vreven, T.; Montgomery, Jr., J. A.; Peralta, J. E.; Ogliaro, F.; Bearpark, M.; Heyd, J. J.; Brothers, E.; Kudin, K. N.; Staroverov, V. N.; Kobayashi, R.; Normand, J.; Raghavachari, K.; Rendell, A.; Burant, J. C.; Iyengar, S. S.; Tomasi, J.; Cossi, M.; Rega, N.; Millam, N. J.; Klene, M.; Knox, J. E.; Cross, J. B.; Bakken, V.; Adamo, C.; Jaramillo, J.; Gomperts, R.; Stratmann, R. E.; Yazyev, O.; Austin, A. J.; Cammi, R.; Pomelli, C.; Ochterski, J.W.; Martin, R. L.; Morokuma, K.; Zakrzewski, V. G.; Voth, G. A.; Salvador, P.; Dannenberg, J. J.; Dapprich, S.; Daniels, A. D.; Farkas, Ö.; Foresman, J. B.; Ortiz, J. V.; Cioslowski, J.; Fox, D. J. (2009): *Gaussian 09, Revision A.1*, Gaussian, Inc., Wallingford CT.

Grätzel, M. (2001): Photoelectrochemical cells. *Nature*, vol. 414, pp. 338-344.

Hara, K.; Kurashige, M. (2003): Design of new coumarin dyes having thiophene moieties for highly efficient organic-dye-sensitized solar cells. *New J. Chem.*, vol. 27, pp. 783-785.

Hong, C. W.; Tsai, C. Y. (2010): Computational quantum mechanics simulation on the photonic properties of group-III nitride clusters. *CMES: Computer Modeling in Engineering & Science*, vol. 67, pp. 79-94.

Hotchandani, S.; Kamat, P. V. (1992): Charge-transfer processes in coupled semiconductor systems: photochemistry and photoelectrochemistry of the colloidal cadmium sulfide-zinc oxide system. *J. Phys. Chem.*, vol. 96, pp. 6834-6839.

Labat, F.; Baranek, P.; Adamo, C. (2008): Structural and electronic properties of selected rutile and anatase TiO₂ surfaces: an ab initio investigation. *J. Chem. Theory Comput.*, vol. 4, pp. 341-352.

Leach, A. R. (2001): *Molecular Modelling Principles and Applications*, 2nd Edition, Prentice Hall, London, U.K.

- Lee, C.; Yang, W.; Parr, R. G.** (1988): Development of the Colle-Salvetti correlation-energy formula into a functional of the electron density. *Phys. Rev. B*, vol. 37, pp. 785-789.
- Lee, H. J.; Yum, J. H.; Leventis, H. C.; Zakeeruddin, S. M.; Haque, S. A.; Chen, P.; Seok, S. I.; Grätzel, M.; Nazeeruddin, M. K.** (2008): CdSe quantum dot-sensitized solar cells exceeding efficiency 1% at full-sun intensity. *J. Phys. Chem. C*, vol. 112, pp. 11600-11608.
- Levine, I. N.** (2009): *Quantum Chemistry*, 6th Edition, Pearson Education, Inc., Upper Saddle River, New Jersey.
- Lewars, E.** (2003): *Computational Chemistry: Introduction to the Theory and Applications of Molecular and Quantum Mechanics*, Klumer Academic Publishers, Dordrecht, The Netherlands.
- Matxain, J. M.; Mercero, J. M.; Fowler, J. E.; Ugalde, J. M.** (2004): Clusters of II-VI materials: Cd_iX_i , $X = S, Se, Te$, $i \leq 16$. *J. Phys. Chem. A*, vol. 108, pp. 10502-10508.
- Mcdonald, S. A.; Konstantatos, G.; Zhang, S.; Cyr, P. W.; Klem, E. J. D.; Levina, L.; Sargent, E. H.** (2005): Solution-processed PbS quantum dot infrared photodetectors and photovoltaics. *Nature Materials*, vol. 4, pp. 138-142.
- Michalet, X.; Pinaud, F. F.; Bentolila, L. A.; Tsay, J. M.; Doose, S.; Li, J. J.; Sundaresan, G.; Wu, A. M.; Gambhir, S. S.; Weiss, S.** (2005): Quantum dots for live cells, in vivo imaging and diagnostics. *Science*, vol. 307, pp. 538-544.
- Perdew, J. P. and Wang, Y.** (1992): Accurate and simple analytic representation of the electron-gas correlation energy. *Phys. Rev. B*, vol. 45, pp. 13244-13249.
- Perdew, J. P.; Chevary, J.A.; Vosko, S. H.; Jackson, K. A.; Pederson, M. R.; Singh, D. J. and Fiolhais, C.** (1992): Atoms, molecules, solids, and surfaces: Applications of the generalized gradient approximation for exchange and correlation. *Phys. Rev. B*, vol. 46, pp. 6671-6687.
- Perdew, J. P.; Burke, K.; Ernzerhof, M.** (1996): Generalized gradient approximation made simple. *Phys. Rev. Lett.*, vol. 77, pp. 3865-3868.
- Peter, L. M.; Riley, D. J.; Tull, E. J.; Wijayantha, K. G. U.** (2002): Photosensitization of nanocrystalline TiO_2 by self-assembled layers of CdS quantum dots. *Chem. Commun.*, vol. 10, pp. 1030-1031
- Plass, R.; Pelet, S.; Krueger, J.; Grätzel, M.** (2002): Quantum dot sensitization of organic-inorganic hybrid solar cells. *J. Phys. Chem. B*, vol. 106, pp. 7578-7580.
- Robel, I.; Subramanian, V.; Kuno, M.; Kamat, P. V.** (2006): Quantum dot solar cells harvesting light energy with CdSe nanocrystals molecularly linked to mesoscopic TiO_2 Films. *J. Am. Chem. Soc.*, vol. 128, pp. 2385-2393.

Schaller, R. D.; Klimov, V. I. (2004): High efficiency carrier multiplication in PbSe nanocrystals: implication for solar energy conversion. *Phys. Rev. Lett.*, vol. 92, pp. 186601-186604.

Srivastava, D.; Atluri, S. N. (2002): Computational nanotechnology: a current perspective. *CMES: Computer Modeling in Engineering & Science*, vol. 3, pp. 531-538.

Tennakone, K.; Kumarasinghe, A.R. (1997): Nanoporous TiO₂ photoanode sensitized with the flower pigment cyanidin. *J. Photochem. Photobiol. A.-Chem.*, vol. 108, pp. 193-195.

Wang, X. F.; Sasaki, S. I. (2010): Chlorophyll-a derivatives with various hydrocarbon ester groups for efficient dye-sensitized solar cells: static and ultrafast evaluations on electron injection and charge collection processes. *Langmuir*, vol. 26, pp. 6320-6327.

Vosko, S. H.; Wilk, L.; Nusair, M. (1980): Accurate spin-dependent electron liquid correlation energies for local spin density calculations: a critical analysis. *Can. J. Phys.* vol. 58, pp. 1200-1211.

Yoshino, K.; Lee, S.; Fujii, A.; Nakayama, H.; Schneider, W.; Naka, A.; Ishikawa, M. (1999): Near IR and UV enhanced photoresponse of C₆₀-doped semiconducting polymer photodiode. *Adv. Mater.*, vol. 11, pp. 1382-1385.

Zeng, H.; Schelly, Z. A.; Noto, K. U.; Marynick, D. S. (2005): Density functional study of structures of lead sulfide clusters (PbS)_n (n = 1-9). *J. Phys. Chem. A*, vol. 109, pp. 1616-1620.